

Modern Physics Letters A  
 © World Scientific Publishing Company

## Top-quark pair production in electron-positron collisions within the minimal noncommutative Standard Model

Fatma Zohra Bara<sup>1,2†</sup>, Slimane Zaiem<sup>2‡\*</sup>, and Yazid Delenda<sup>1,2¶</sup>

<sup>1</sup>*Laboratoire de Physique des Rayonnements et de leurs Interactions avec la Matière,*

<sup>2</sup>*Département de Physique, Faculté des Sciences de la Matière,*

*Université de Batna-1, Batna 05000, Algeria*

<sup>†</sup>*fatmazohra.bara@univ-batna.dz*

<sup>‡</sup>*slimane.zaiem@univ-batna.dz*

<sup>¶</sup>*yazid.delenda@univ-batna.dz*

We study top-quark pair production in electron-positron collisions within the framework of the minimal noncommutative Standard Model. Noncommutative effects are incorporated using the Seiberg-Witten map, and the scattering squared amplitude for the process  $e^+e^- \rightarrow t\bar{t}$  is computed consistently up to second order in the noncommutativity parameter  $\Theta^{\mu\nu}$ . We derive the total cross-section, the polar and azimuthal angular distributions, and the forward-backward asymmetry, all of which exhibit sensitivity to space-time noncommutativity. Numerical results are evaluated for center-of-mass energies relevant to future linear colliders, such as the ILC and CLIC. Our analysis demonstrates that noncommutative geometry can induce significant characteristic deviations from the Standard Model predictions, offering a potential indirect probe of space-time noncommutativity at high-energy  $e^+e^-$  collisions.

*Keywords:* Noncommutative Standard Model, top-quark physics,  $e^+e^-$  collisions, forward-backward asymmetry.

PACS Nos.: 11.10.Nx, 14.65.Ha, 13.66.Jn, 12.60.-i

### 1. Introduction

The discovery of the Higgs boson at the Large Hadron Collider (LHC) [1,2] marked a triumph of the Standard Model (SM), yet several fundamental questions remain unanswered. Among these are the nature of electroweak symmetry breaking, the origin of the observed fermion mass hierarchy, and the notably large mass of the top quark. These unresolved issues indicate that the SM is not a complete theory and motivate the search for physics Beyond the Standard Model (BSM), which has become a central focus of high-energy physics. Promising theoretical frameworks include supersymmetry [3,4], extra dimensions [5–8], and noncommutative geometry [9], each predicting new phenomena that could be accessible at current and future colliders.

\*Corresponding author.

The top quark, with a mass near the electroweak scale, serves as a unique probe for BSM physics due to its strong coupling to the Higgs sector and potential sensitivity to new interactions. Precision studies of top-quark production and decay are therefore central to the physics programs of present and future colliders. Electron-positron colliders offer a particularly clean environment for such studies, with well-defined initial states and reduced QCD backgrounds compared to hadron colliders. Future facilities such as the International Linear Collider (ILC) [10, 11], the Compact Linear Collider (CLIC) [12], and others like the FCC-ee [13] and CEPC [14], are expected to operate at energies well above the top-pair threshold and reaching the TeV scale, enabling high-precision measurements of cross-sections, angular distributions, and asymmetries as well as searches for new physics signals, exploring the plethora of models that complement the SM.

Among these many BSM scenarios, Noncommutative (NC) geometry provides an intriguing extension of space-time structure, where coordinates  $\hat{x}^\mu$  satisfy a non-trivial commutation relation

$$[\hat{x}^\mu, \hat{x}^\nu] = i \Theta^{\mu\nu} = \frac{i}{\Lambda_{\text{NC}}^2} C^{\mu\nu}, \quad (\mu, \nu = 0, 1, 2, 3), \quad (1)$$

where  $\Theta^{\mu\nu}$  is an antisymmetric constant tensor encoding the scale and structure of noncommutativity. The idea of quantized space-time dates back to Snyder's early work [15], and such a structure emerges naturally in certain limits of string theory [16, 17] and quantum gravity models. This idea leads to distinctive corrections to quantum field theories defined on NC space-time, and has thus sparked considerable interest in the NC nature of space-time on the TeV-scale within the particle physics community. Using the Seiberg-Witten (SW) map, Calmet et al. [18] constructed the minimal Noncommutative Standard Model (mNCSM) as a consistent gauge theory on noncommutative space-time. In this framework, NC corrections appear as gauge-invariant higher-dimensional operators suppressed by  $\Lambda_{\text{NC}}$ . To avoid potential issues with unitarity and causality [17, 19, 20], one typically restricts to purely space-space noncommutativity ( $\Theta^{0i} = 0$ ), though space-time components can also be considered with careful treatment.

In canonical NC field theory, ordinary products are replaced by the Moyal-Weyl star product

$$(f \star g)(x) = \exp\left(\frac{i}{2} \Theta^{\mu\nu} \frac{\partial}{\partial x^\mu} \frac{\partial}{\partial y^\nu}\right) f(x) g(y) \Big|_{y \rightarrow x}, \quad (2)$$

which, however, introduces challenges such as UV/IR mixing [19, 21]. A more robust approach uses the SW map, which expresses NC fields as expansions in  $\Theta$  of their commutative counterparts, thus preserving gauge invariance and enabling the construction of realistic models, with demonstrated progress in perturbative renormalization [22, 23].

Phenomenological studies within the mNCSM have already set preliminary bounds on the NC scale  $\Lambda_{\text{NC}}$  [4, 24–31]. For instance, analyses of  $ZZ/\gamma\gamma$  [28],

$W^+W^-$  [29], and Drell–Yan processes [30] via exotic photon-gluon-gluon and  $Z$ -gluon-gluon interactions at the LHC have yielded limits in the range  $\Lambda_{\text{NC}} \gtrsim 0.4\text{--}1 \text{ TeV}$ . For top-quark pair production in  $e^+e^-$  collisions, earlier mNCSM studies using first-order expansions in  $\Theta$  obtained bounds around  $\Lambda_{\text{NC}} \sim 0.1\text{--}0.2 \text{ TeV}$  [26], while more recent analyses of angular asymmetries have pushed the sensitivity to  $\Lambda_{\text{NC}} \sim 1\text{--}2.8 \text{ TeV}$  using polarized beams and non-minimal couplings [25, 31].

In this work, we extend these analyses by computing the scattering squared amplitude for  $e^+e^- \rightarrow t\bar{t}$  within the mNCSM consistently up to second order in  $\Theta^{\mu\nu}$  using the SW map approach. We provide comprehensive analytical results for the total and differential cross-sections, including polar and azimuthal distributions and the forward-backward asymmetry. Special attention is given to space-time non-commutativity, which induces characteristic directional dependencies in angular observables. Numerical evaluations are performed for center-of-mass energies relevant to the ILC and CLIC, and lower bounds on  $\Lambda_{\text{NC}}$  are derived based on sensitivity estimates, and the collision threshold energy required to observe these NC effects is established.

The paper is organized as follows. In section 2, we present the squared amplitude for  $e^+e^- \rightarrow t\bar{t}$  in the mNCSM. Section 3 details the kinematics and parameterization of NC deformations. Section 4 contains numerical results for total and angular distributions, as well as the forward-backward asymmetry. Section 5 summarizes our findings and outlines prospects for future collider searches.

## 2. Squared amplitude for the process $e^+e^- \rightarrow \gamma/Z \rightarrow t\bar{t}$ in the mNCSM

We consider the pair production of top quarks in electron-positron annihilation,  $e^-(p_1)e^+(p_2) \rightarrow t(p_3)\bar{t}(p_4)$ , which proceeds through an  $s$ -channel exchange of a photon and a  $Z$  boson within the framework of the mNCSM. The corresponding Feynman diagrams are shown in figure 1. In order to consistently compute the cross section including NC effects, we employ the Feynman rules expanded up to first order in the noncommutativity parameter  $\Theta_{\mu\nu}$ . Details of the relevant Feynman rules are provided in Appendix A.

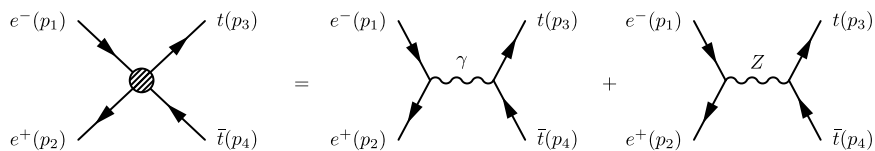


Fig. 1. Feynman diagrams for the process  $e^-e^+ \rightarrow \gamma/Z \rightarrow t\bar{t}$  in the mNCSM.

Up to  $\mathcal{O}(\Theta)$ , the scattering amplitudes for photon- and  $Z$ -boson exchange can

be written in a factorized form as

$$i A_{\gamma/Z} = i A_{\gamma/Z}^{\text{SM}} \left( 1 + \frac{i}{2} p_2 \Theta p_1 \right) \left( 1 + \frac{i}{2} p_3 \Theta p_4 \right), \quad (3a)$$

$$i A_{\gamma}^{\text{SM}} = -\frac{8\pi\alpha i}{3s} [\bar{v}(p_2)\gamma_{\mu}u(p_1)] [\bar{u}(p_3)\gamma^{\mu}v(p_4)], \quad (3b)$$

$$\begin{aligned} i A_Z^{\text{SM}} = & \frac{4\pi\alpha i}{\sin^2(2\theta_w)(s-m_Z^2+im_Z\Gamma_Z)} [\bar{v}(p_2)\gamma_{\mu}(c_V^e - c_A^e\gamma_5)u(p_1)] \\ & \times [\bar{u}(p_3)\gamma^{\mu}(c_V^t - c_A^t\gamma_5)v(p_4)]. \end{aligned} \quad (3c)$$

Here we use the shorthand notation  $p_i\Theta p_j \equiv p_i^{\mu}\Theta_{\mu\nu}p_j^{\nu}$ ,  $s = (p_1 + p_2)^2$  denotes the squared centre-of-mass energy, and  $\alpha = e^2/(4\pi)$  is the QED coupling constant. The vector and axial-vector couplings of a fermion  $i$  are given by

$$c_V^i = T_3^i - 2Q_i \sin^2 \theta_w, \quad c_A^i = T_3^i, \quad (4)$$

where  $T_3^i$  and  $Q_i$  are the weak isospin and electric charge of the fermion, respectively, and  $\theta_w$  is the Weinberg mixing angle. The quantities  $m_Z$  and  $\Gamma_Z$  denote the mass and total decay width of the  $Z$  boson.

After summing over final-state spins and colors and averaging over the initial-state spins, the squared amplitude for the process  $e^+e^- \rightarrow t\bar{t}$  can be written in the compact form

$$\overline{|\mathcal{A}|^2} = \overline{|\mathcal{A}^{\text{SM}}|^2} (1 + \mathcal{N}), \quad (5)$$

where  $\mathcal{N}$  encodes the leading NC correction. To  $\mathcal{O}(\Theta^2)$ , this correction factor is given by

$$\mathcal{N} = \frac{1}{4} (p_2 \Theta p_1)^2 + \frac{1}{4} (p_3 \Theta p_4)^2 + \mathcal{O}(\Theta^4). \quad (6)$$

The SM contribution can be decomposed into pure photon, pure  $Z$ , and  $\gamma$ - $Z$  interference terms as

$$\overline{|\mathcal{A}^{\text{SM}}|^2} = \overline{|\mathcal{A}_{\gamma}^{\text{SM}}|^2} + \overline{|\mathcal{A}_Z^{\text{SM}}|^2} + 2 \text{Re} \left( \overline{\mathcal{A}_{\gamma}^{\text{SM}*} \mathcal{A}_Z^{\text{SM}}} \right). \quad (7)$$

Explicitly, these contributions read

$$\overline{|\mathcal{A}_{\gamma}^{\text{SM}}|^2} = \frac{128}{3} \pi^2 \alpha^2 \left[ \frac{t^2 + u^2}{s^2} + 4 \frac{m_t^2}{s} \left( 1 - \frac{m_t^2}{2s} \right) \right], \quad (8a)$$

$$\begin{aligned} \overline{|\mathcal{A}_Z^{\text{SM}}|^2} = & \frac{96\pi^2\alpha^2}{\sin^4(2\theta_w)} \frac{s^2}{(s-m_Z^2)^2+m_Z^2\Gamma_Z^2} \left[ 4 c_A^e c_A^t c_V^e c_V^t \frac{t-u}{s} \right. \\ & \left. + (c_A^e)^2 + (c_V^e)^2 \right] (c_A^t)^2 + c_V^t \left( \frac{t^2+u^2}{s^2} + 4 \frac{m_t^2}{s} \left( \frac{c_V^t}{c_V^t + c_A^t} - \frac{m_t^2}{2s} \right) \right) \left. \right], \end{aligned} \quad (8b)$$

$$\begin{aligned} 2 \text{Re} \left( \overline{\mathcal{A}_{\gamma}^{\text{SM}*} \mathcal{A}_Z^{\text{SM}}} \right) = & -\frac{128\pi^2\alpha^2}{\sin^2(2\theta_w)} \frac{s(s-m_Z^2)}{(s-m_Z^2)^2+m_Z^2\Gamma_Z^2} \\ & \times \left[ c_V^e c_V^t \left( \frac{t^2+u^2}{s^2} + 4 \frac{m_t^2}{s} \left( 1 - \frac{m_t^2}{2s} \right) \right) + c_A^e c_A^t \frac{t-u}{s} \right]. \end{aligned} \quad (8c)$$

Here  $t = (p_1 - p_3)^2$  and  $u = (p_1 - p_4)^2$  are the usual Mandelstam variables, and  $m_t$  denotes the top-quark mass. We ignore the electron mass at high energies.

In the following sections, these results are employed to compute the total cross section as well as the angular distributions for the process  $e^+e^- \rightarrow t\bar{t}$  in the mNCSM.

### 3. Kinematics and choices of deformation

In this work we present predictions for both total and differential cross sections for the process  $e^+e^- \rightarrow t\bar{t}$  in NC geometry. The differential angular distribution  $d\sigma/d\Omega$  is obtained by integrating the spin- and color-summed squared amplitude over the full phase space of the anti-top momentum  $p_4$  and over the magnitude of the top-quark three-momentum  $|\mathbf{p}_3|$ , while keeping the polar and azimuthal angles  $(\theta, \phi)$  of the top quark unintegrated. The solid-angle element is  $d\Omega = d\cos\theta d\phi$ . The total cross section then follows from

$$\sigma = \int_{-1}^1 d\cos\theta \int_0^{2\pi} d\phi \frac{d\sigma}{d\Omega}. \quad (9)$$

After performing the phase-space integrations and imposing on-shell conditions together with four-momentum conservation, the differential angular distribution can be expressed in terms of the squared matrix element as

$$\frac{d\sigma}{d\Omega} = \frac{1}{64\pi^2 s} \sqrt{1 - \frac{4m_t^2}{s}} |\mathcal{A}|^2. \quad (10)$$

All cross sections are evaluated in the center-of-mass frame, where the produced  $t\bar{t}$  pair is back-to-back. The four-momenta of the incoming and outgoing particles are chosen as

$$p_1 = \frac{\sqrt{s}}{2} (1, 0, 0, 1), \quad (11a)$$

$$p_2 = \frac{\sqrt{s}}{2} (1, 0, 0, -1), \quad (11b)$$

$$p_3 = \frac{\sqrt{s}}{2} (1, k \sin\theta \cos\phi, k \sin\theta \sin\phi, k \cos\theta), \quad (11c)$$

$$p_4 = \frac{\sqrt{s}}{2} (1, -k \sin\theta \cos\phi, -k \sin\theta \sin\phi, -k \cos\theta), \quad (11d)$$

with

$$k = \sqrt{1 - 4 \frac{m_t^2}{s}}. \quad (12)$$

In this parametrization the Mandelstam variables reduce to

$$t = m_t^2 - \frac{s}{2} (1 - k \cos\theta), \quad (13a)$$

$$u = m_t^2 - \frac{s}{2} (1 + k \cos\theta). \quad (13b)$$

In the NC extension of the SM, the antisymmetric tensor  $\Theta^{\mu\nu}$  contains six independent parameters in four-dimensional space-time. It can be decomposed into

space-time and space-space components,  $\Theta^{0i}$  and  $\Theta^{ij}$  ( $i, j = 1, 2, 3$ ), which are conveniently parametrized in terms of a characteristic NC scale  $\Lambda_{\text{NC}}$  and two dimensionless vectors  $\xi$  and  $\beta$  as

$$\Theta^{0i} = \frac{1}{\Lambda_{\text{NC}}^2} \xi_i, \quad (14a)$$

$$\Theta^{ij} = \frac{1}{\Lambda_{\text{NC}}^2} \epsilon_{ijk} \beta^k. \quad (14b)$$

The structure of  $\Theta^{\mu\nu}$  is formally analogous to that of the electromagnetic field strength tensor, with  $\xi$  and  $\beta$  playing the role of effective electric- and magnetic-like components, respectively. In the context of a simplified isotropic scenario, these parameters are set as  $\xi_i = \beta_i = 1/\sqrt{3}$ . Anisotropic NC space-times with variable  $\xi_i$  and  $\beta_i$  are equally physically admissible.

While purely space-space noncommutativity preserves unitarity and causality at the perturbative level, it leads to a strong suppression of observable effects in many  $2 \rightarrow 2$  scattering processes. In particular, for  $s$ -channel reactions such as  $e^+e^- \rightarrow t\bar{t}$ , the leading NC corrections proportional to  $(p_2\Theta p_1)$  and  $(p_3\Theta p_4)$  vanish identically in the center-of-mass frame when only  $\Theta^{ij}$  is nonzero. Consequently, purely space-space noncommutativity fails to generate any deviation from the SM prediction at leading order, rendering this scenario phenomenologically uninformative for collider studies for the particular process of interest in this paper.

Allowing for space-time noncommutativity ( $\Theta^{0i} \neq 0$ ) restores nonvanishing leading-order corrections and induces characteristic polar and azimuthal modulations in angular observables. It is well known, however, that space-time noncommutativity generically leads to an apparent violation of perturbative unitarity, manifested by a rapid growth of total cross sections with increasing center-of-mass energy. Within the framework of the mNCSM, this behavior should be interpreted as signaling the breakdown of the effective field-theory (EFT) description near the NC scale  $\Lambda_{\text{NC}}$ , rather than as a fundamental inconsistency of the underlying theory.

Since the mNCSM is constructed as an EFT expanded in powers of the noncommutativity parameter  $\Theta \sim \Lambda_{\text{NC}}^{-2}$ , perturbative control requires the dimensionless expansion parameter  $s/\Lambda_{\text{NC}}^2$  not to be parametrically large. In practice, phenomenologically relevant NC effects arise when  $\Lambda_{\text{NC}}$  is of the same order as the collider energy  $\sqrt{s}$ . For  $\Lambda_{\text{NC}} \gg \sqrt{s}$  the NC-induced deviations rapidly become suppressed and phenomenologically unobservable, while for  $\Lambda_{\text{NC}} \ll \sqrt{s}$  the EFT description ceases to be reliable. Accordingly, meaningful phenomenological analyses should focus on the intermediate regime  $\Lambda_{\text{NC}} \gtrsim \sqrt{s}$  and primarily on differential observables, such as polar and azimuthal angular distributions, where NC effects arise through interference with the SM amplitudes and remain under qualitative perturbative control.

In this study we parameterize the space-time NC tensor as

$$\Theta^{\mu\nu} = \frac{1}{\Lambda_{\text{NC}}^2} \begin{pmatrix} 0 & \xi_x & \xi_y & \xi_z \\ -\xi_x & 0 & 0 & 0 \\ -\xi_y & 0 & 0 & 0 \\ -\xi_z & 0 & 0 & 0 \end{pmatrix}, \quad (15)$$

where the dimensionless unit vector  $(\xi_x, \xi_y, \xi_z)$  specifies the orientation of the space-time deformation, in analogy with an electric-field direction. The inclusion of additional space-space components does not affect our results. For a general space-time deformation, the NC correction factor introduced in eq. (6) can be written as

$$\mathcal{N} = \frac{s^2}{16 \Lambda_{\text{NC}}^4} \left[ \xi_z^2 + \left( 1 - 4 \frac{m_t^2}{s} \right) (\xi_z \cos \theta + \xi_x \sin \theta \cos \phi + \xi_y \sin \theta \sin \phi)^2 \right]. \quad (16)$$

In the following we specialize to the discussion of two representative scenarios: (i) a transverse deformation in the plane perpendicular to the beam axis,  $(\xi_x, \xi_y, 0)$ , for which

$$\mathcal{N}_T = \frac{s^2}{16 \Lambda_{\text{NC}}^4} \left( 1 - 4 \frac{m_t^2}{s} \right) \sin^2 \theta (\xi_x \cos \phi + \xi_y \sin \phi)^2, \quad (17)$$

and (ii) a purely longitudinal deformation along the beam direction,  $(0, 0, \xi_z)$  with  $\xi_z = 1$ , leading to

$$\mathcal{N}_L = \frac{s^2}{16 \Lambda_{\text{NC}}^4} \left[ 1 + \left( 1 - 4 \frac{m_t^2}{s} \right) \cos^2 \theta \right]. \quad (18)$$

These two benchmark choices capture the essential qualitative features of NC effects in the angular distributions of the  $e^+e^- \rightarrow t\bar{t}$  process.

#### 4. Total and angular differential cross-sections

##### 4.1. Total cross-section

We begin by examining the impact of NC geometry on the total cross section. After averaging over the azimuthal angle, the NC correction factor takes the form

$$\int_0^{2\pi} \mathcal{N} d\phi = \frac{s^2}{16 \Lambda_{\text{NC}}^4} 2\pi \left[ \xi_z^2 + \left( 1 - 4 \frac{m_t^2}{s} \right) \left( \xi_z^2 \cos^2 \theta + \frac{1}{2} (\xi_x^2 + \xi_y^2) \sin^2 \theta \right) \right]. \quad (19)$$

Upon integration over the polar angle, the total cross section can be written as

$$\sigma = \sigma_{\text{SM}} + \delta\sigma_{\text{NC}}, \quad (20)$$

where  $\sigma_{\text{SM}}$  denotes the SM contribution and  $\delta\sigma_{\text{NC}}$  encodes the NC correction.

The SM total cross section is given by

$$\begin{aligned} \sigma^{\text{SM}} = & \frac{4\pi\alpha^2}{s} \sqrt{1 - 4 \frac{m_t^2}{s}} \left\{ \frac{4}{9} \left( 1 + 2 \frac{m_t^2}{s} \right) \right. \\ & + \frac{c_A^e + c_V^e}{\sin^4(2\theta_w)} \frac{s^2}{(s - M_Z^2)^2 + \Gamma_Z^2 M_Z^2} \left[ c_A^{t2} \left( 1 - 4 \frac{m_t^2}{s} \right) + c_V^{t2} \left( 1 + 2 \frac{m_t^2}{s} \right) \right] \\ & \left. - \frac{4}{3} \frac{c_V^e c_V^t}{\sin^2(2\theta_w)} \frac{s(s - M_Z^2)}{(s - M_Z^2)^2 + \Gamma_Z^2 M_Z^2} \left( 1 + 2 \frac{m_t^2}{s} \right) \right\}. \end{aligned} \quad (21)$$

The NC contribution can be decomposed into longitudinal and transverse components,

$$\delta\sigma_{\text{NC}} = \delta\sigma_L^{\text{NC}} + \delta\sigma_T^{\text{NC}}, \quad (22)$$

corresponding to deformations parallel and perpendicular to the beam axis, respectively.

For Longitudinal space-time deformations, the NC correction reads

$$\begin{aligned} \delta\sigma_L^{\text{NC}} = & \xi_z^2 \frac{s^2}{80 \Lambda_{\text{NC}}^4} \frac{4\pi\alpha^2}{s} \sqrt{1 - 4 \frac{m_t^2}{s}} \left\{ \frac{4}{9} \left( 7 + 4 \frac{m_t^2}{s} - 8 \frac{m_t^4}{s^2} \right) \right. \\ & + \frac{c_A^e + c_V^e}{\sin^4(2\theta_w)} \frac{s^2}{(s - M_Z^2)^2 + \Gamma_Z^2 M_Z^2} \\ & \times \left[ 7(c_V^{t2} + c_A^{t2}) + 4 \frac{m_t^2}{s} (c_V^{t2} - 9c_A^{t2}) - 8 \frac{m_t^4}{s^2} (c_V^{t2} - 4c_A^{t2}) \right] \\ & \left. - \frac{4}{3} \frac{c_V^e c_V^t}{\sin^2(2\theta_w)} \frac{s(s - M_Z^2)}{(s - M_Z^2)^2 + \Gamma_Z^2 M_Z^2} \left( 7 + 4 \frac{m_t^2}{s} - 8 \frac{m_t^4}{s^2} \right) \right\}, \end{aligned} \quad (23)$$

and for transverse space-time deformations one obtains

$$\begin{aligned} \delta\sigma_T^{\text{NC}} = & (\xi_x^2 + \xi_y^2) \frac{s^2}{160 \Lambda_{\text{NC}}^4} \frac{4\pi\alpha^2}{s} \sqrt{1 - 4 \frac{m_t^2}{s}} \left\{ \frac{4}{9} \left( 1 - 4 \frac{m_t^2}{s} \right) \left( 3 + 8 \frac{m_t^2}{s} \right) \right. \\ & + \frac{c_A^e + c_V^e}{\sin^4(2\theta_w)} \frac{s^2}{(s - M_Z^2)^2 + \Gamma_Z^2 M_Z^2} \\ & \times \left( 1 - 4 \frac{m_t^2}{s} \right) \left[ 3c_A^{t2} \left( 1 - 4 \frac{m_t^2}{s} \right) + c_V^{t2} \left( 3 + 8 \frac{m_t^2}{s} \right) \right] \\ & \left. - \frac{4}{3} \frac{c_V^e c_V^t}{\sin^2(2\theta_w)} \frac{s(s - M_Z^2)}{(s - M_Z^2)^2 + \Gamma_Z^2 M_Z^2} \left( 1 - 4 \frac{m_t^2}{s} \right) \left( 3 + 8 \frac{m_t^2}{s} \right) \right\}. \end{aligned} \quad (24)$$

In figure 2 we display the total cross section as a function of the center-of-mass energy  $\sqrt{s}$ , ranging from 0.35 TeV to 3 TeV, covering the energy reach of future  $e^+e^-$  colliders such as the FCC-ee, ILC, and CLIC. The results are shown for several values of the NC scale  $\Lambda_{\text{NC}}$  and for both transverse and longitudinal space-time deformations. Throughout, we use  $m_t = 173$  GeV.

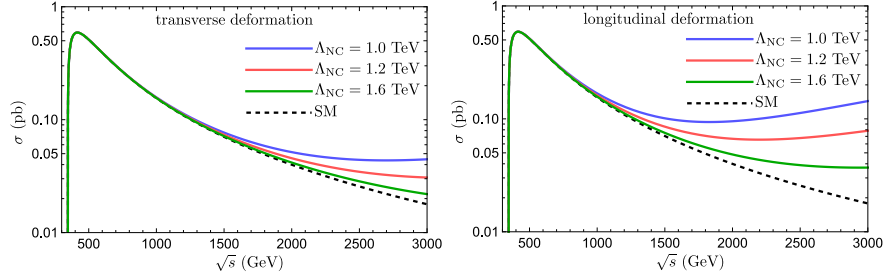


Fig. 2. Total cross-section for transverse (left) and longitudinal (right) space-time deformations as a function of the center-of-mass energy  $\sqrt{s}$ .

In contrast to purely space-space noncommutativity, which typically suppresses the cross section in other processes, space-time noncommutativity leads to an enhancement that grows with  $\sqrt{s}$ . This enhancement becomes more pronounced for smaller values of  $\Lambda_{\text{NC}}$ , and is particularly strong for longitudinal deformations with  $\xi = (0, 0, 1)$ .

Higher center-of-mass energies therefore provide an effective probe of TeV-scale space-time NC deformations, where modest deviations from the SM prediction may signal physics beyond the SM. For example, at  $\sqrt{s} = 3$  TeV the SM prediction for  $\sigma(e^+e^- \rightarrow t\bar{t})$  is approximately 0.018 pb. A transverse NC deformation shifts this value to about 0.022 pb, corresponding to an enhancement of roughly 23% for  $\Lambda_{\text{NC}} = 1.6$  TeV, while longitudinal deformations can lead to enhancements exceeding 100% at the same scale. Consequently, precision measurements at future  $e^+e^-$  colliders could realistically exclude NC scales in the TeV range and potentially extend sensitivity into the multi-TeV regime. Similar conclusions were reached in ref. [32] for Higgs-pair production in the NCSM.

To further quantify NC effects, we show in figure. 3 the NC correction  $\delta\sigma_{\text{NC}}$  as a function of  $\sqrt{s}$  for different values of  $\Lambda_{\text{NC}}$ , and as a function of  $\Lambda_{\text{NC}}$  for fixed  $\sqrt{s}$ , in the case of transverse deformations. These results confirm that NC effects decrease

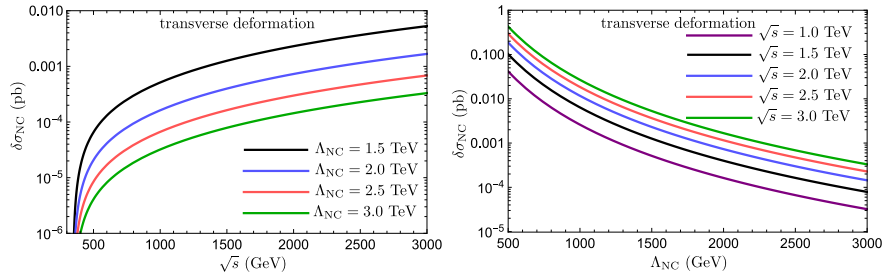


Fig. 3. NC correction to the total cross-section for transverse space-time deformations as a function of the center-of-mass energy  $\sqrt{s}$  (left) and of the NC scale  $\Lambda_{\text{NC}}$  (right).

with increasing  $\Lambda_{\text{NC}}$  and grow with  $\sqrt{s}$ , highlighting the importance of high-energy collisions for probing NC geometry.

#### 4.1.1. Collision threshold energy

We adopt a *detection-threshold* strategy and introduce a benchmark collision energy  $\sqrt{s_0}$ , defined as the minimum machine centre-of-mass energy required for the NC contribution to the cross section,  $\delta\sigma_{\text{NC}}$ , to reach a fixed fraction  $p$  of the corresponding SM prediction. Explicitly,  $\sqrt{s_0}$  is determined by the condition

$$\frac{\delta\sigma_{\text{NC}}(\sqrt{s_0})}{\sigma_{\text{SM}}(\sqrt{s_0})} = p, \quad (25)$$

where we take  $p = 10\%$  for illustrative purposes. This choice represents a conservative benchmark corresponding to a measurable deviation that could plausibly yield a  $5\sigma$  indication of NC effects in precision cross-section measurements.

For a fixed value of the NC scale  $\Lambda_{\text{NC}}$ , the threshold energy  $\sqrt{s_0}$  is obtained by numerically solving eq. (25). The resulting values of  $\sqrt{s_0}$  as a function of  $\Lambda_{\text{NC}}$  are displayed in figure 4. The numerical data exhibit an approximately linear dependence between the two quantities over the range of parameters considered.

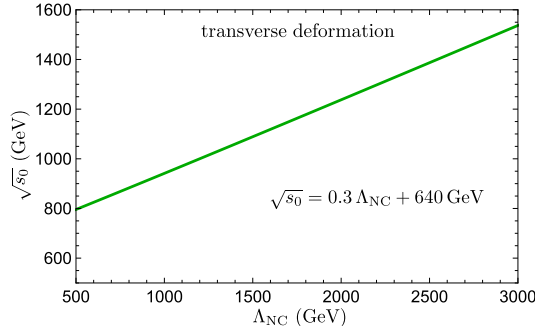


Fig. 4. Threshold centre-of-mass energy  $\sqrt{s_0}$  as a function of the NC scale  $\Lambda_{\text{NC}}$  for transverse space-time deformations.

To quantify this behaviour, we perform a linear interpolation of the numerical results shown in figure 4. This yields the following empirical parametrization for the threshold energy,

$$\sqrt{s_0} = \mathcal{A} \Lambda_{\text{NC}} + \mathcal{B}, \quad \mathcal{A} = 0.3, \quad \mathcal{B} = 640 \text{ GeV}. \quad (26)$$

This result indicates that, as the NC scale increases, the required minimum centre-of-mass energy grows more slowly, at a rate of roughly 30% of the growth of  $\Lambda_{\text{NC}}$ . Consequently, relatively modest increases in collider energy are sufficient to probe significantly larger values of the NC scale.

The primary significance of this parametrization lies in its direct applicability as a predictive tool for future experimental programs. For example, if theoretical considerations point to an NC scale of order  $\Lambda_{\text{NC}} \simeq 3.0$  TeV, our relation predicts a minimum centre-of-mass energy of approximately  $\sqrt{s_0} \simeq 1.5$  TeV to reach the target sensitivity. Conversely, the absence of an observed deviation at a given collider energy can be immediately translated into a lower bound on  $\Lambda_{\text{NC}}$ . In this way, eq (26) provides a transparent framework for both discovery-oriented searches and the interpretation of null results, hence offering clear guidance for future investigations of NC effects in the top-quark sector.

#### 4.2. Polar distribution and forward-backward asymmetry

Turning to differential observables, we now analyze the polar-angle distribution of the top quark together with the associated forward-backward asymmetry. As in the case of the total cross section, azimuthal averaging decomposes the differential distribution into longitudinal and transverse components, as given in eq. (19). Employing this azimuthal-averaged NC correction, we compute and display the differential polar distribution  $d\sigma/d\cos\theta$  as a function of  $\cos\theta$  in figure 5. The results are shown for several representative values of the NC scale  $\Lambda_{\text{NC}}$ , at centre-of-mass energies  $\sqrt{s} = 1$  TeV and  $\sqrt{s} = 3$  TeV, and for both transverse and longitudinal deformations of space-time noncommutativity. The chosen values of  $\Lambda_{\text{NC}}$  are taken sufficiently large compared to  $\sqrt{s}$  in order to avoid the unitarity issues discussed previously.

As can be seen from the figure, the polar-angle distributions exhibit a pronounced sensitivity to the NC scale when  $\Lambda_{\text{NC}}$  is of the same order as the collider energy  $\sqrt{s}$ . For example, at CLIC energies ( $\sqrt{s} = 3$  TeV), a longitudinal NC deformation with  $\Lambda_{\text{NC}} = 2.5$  TeV induces corrections at the level of  $\sim 25\%$  in the forward region,  $\cos\theta \simeq 1$ . A comparable modification, of order  $\sim 28\%$ , is obtained at ILC energies ( $\sqrt{s} = 1$  TeV) for a smaller NC scale,  $\Lambda_{\text{NC}} = 0.8$  TeV. In contrast, transverse deformations primarily affect the central region of the distribution around  $\cos\theta \simeq 0$ , where the induced deviations are more modest, reaching the level of approximately 6-7% for the said energy scales.

The asymmetry of the polar-angle distribution can be quantified more precisely by the top-quark forward-backward asymmetry, defined as

$$A_{\text{FB}}^t = \frac{\sigma_{\text{forward}} - \sigma_{\text{backward}}}{\sigma_{\text{forward}} + \sigma_{\text{backward}}}, \quad (27)$$

where  $\sigma_{\text{forward}}$  [ $\sigma_{\text{backward}}$ ] is obtained by integrating the differential distribution over the forward ( $0 < \cos\theta < 1$ ) [backward ( $-1 < \cos\theta < 0$ )] hemisphere. This observable is well known for its sensitivity to deviations from the SM and is widely employed in experimental analyses as a sensitive probe in searches for new physics scenarios.

In figure 6 we present  $A_{\text{FB}}^t$  as a function of the centre-of-mass energy. Within the SM, the forward production of top quarks is strongly enhanced, with the asymmetry

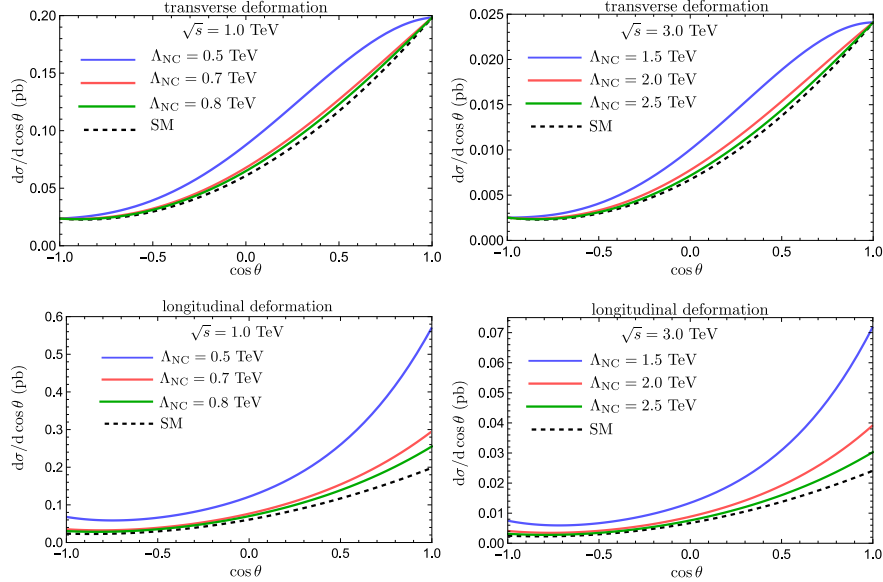


Fig. 5. Differential polar-angle distribution of the top quark for transverse (top panels) and longitudinal (bottom panels) NC deformations.

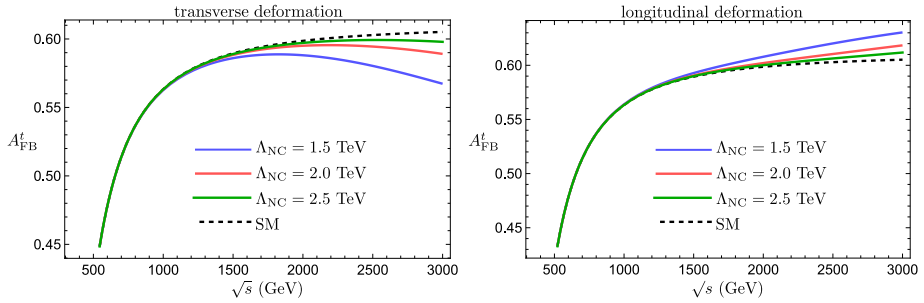


Fig. 6. Forward-backward asymmetry of the top quark for transverse (left) and longitudinal (right) NC deformations.

rising with  $\sqrt{s}$  and reaching values of about 0.6 at  $\sqrt{s} = 3$  TeV, eventually saturating at approximately 0.61 at very high energies. NC corrections have a significant impact on this behaviour: transverse deformations tend to reduce the forward-backward asymmetry, while longitudinal deformations enhance it.

Quantitatively, at  $\sqrt{s} = 3$  TeV and for  $\Lambda_{\text{NC}} = 2.5$  TeV, we find a downward (upward) shift of the asymmetry at the level of  $\sim 1\%$  for transverse (longitudinal) deformations. More generally, a collider operating at this energy would be sensitive to NC scales of order  $\Lambda_{\text{NC}} \sim 1.5$  TeV, provided experimental uncertainties can be controlled at the 5% level, corresponding to deviations of this magnitude from the

SM prediction. The experimental capabilities of a machine such as CLIC—including its high integrated luminosity at the inverse-attobarn level, excellent detector performance, and clean event reconstruction—make precision measurements of this kind feasible. Such measurements could either impose stringent constraints on the NC scale or provide the first hints of its possible existence in the top-quark sector.

#### 4.3. Azimuthal modulation

Within the SM, the azimuthal-angle distribution of the produced top quark is strictly flat, reflecting the rotational symmetry of the underlying dynamics around the beam axis. In contrast, NC effects introduce additional momentum-dependent structures in the squared matrix element, thus breaking this isotropy. As a result, the azimuthal distribution constitutes a particularly sensitive observable for probing space-time noncommutativity and has been widely exploited in phenomenological studies of this kind.

In the case of space-time noncommutativity, the NC correction factor  $\mathcal{N}$  acquires an explicit dependence on the azimuthal angle through the transverse components of the deformation vector  $\xi$ . Consequently, purely longitudinal deformations lead only to an overall rescaling of the azimuthal distribution, leaving its shape unchanged. By contrast, for purely transverse deformations, the functional form of  $\mathcal{N}$  implies a characteristic sinusoidal modulation of the azimuthal distribution, with an amplitude and phase governed by the deformation factor given in eq. (17).

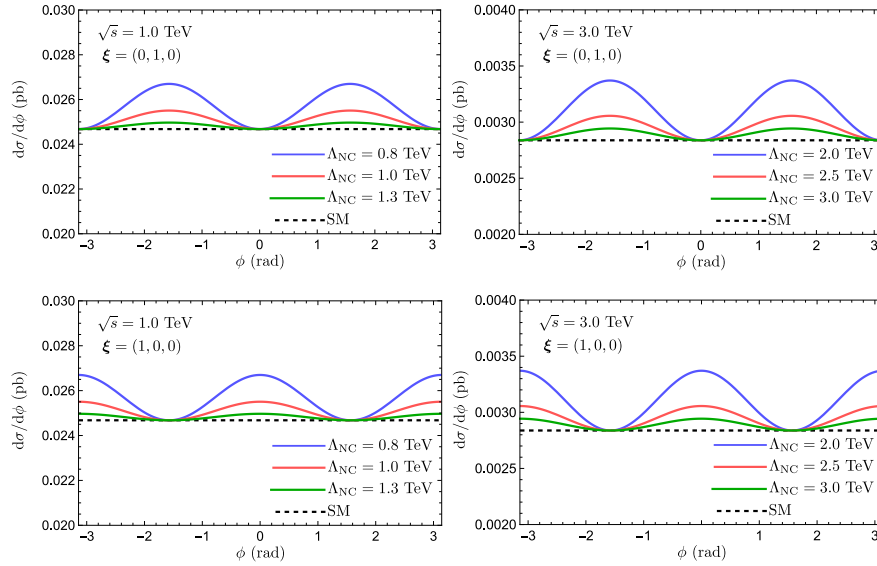


Fig. 7. Differential azimuthal-angle distribution for transverse deformations along the  $y$  axis (top) and the  $x$  axis (bottom).

In figure 7, we present the differential azimuthal distribution  $d\sigma/d\phi$  as a function of the azimuthal angle  $\phi$  at centre-of-mass energies  $\sqrt{s} = 1$  TeV and  $\sqrt{s} = 3$  TeV, for transverse deformations oriented along the  $x$  and  $y$  axes. Deformations in the transverse plane induce a smooth phase shift when moving from an  $x$ -axis to a  $y$ -axis deformation, directly reflecting the sinusoidal structure of the NC correction factor in Eq. (17).

The impact of space-time noncommutativity on this distribution is particularly pronounced at higher energies. Focusing on  $\sqrt{s} = 3$  TeV, we find that for a NC scale of  $\Lambda_{\text{NC}} = 3$  TeV the azimuthal distribution is distorted by up to approximately 4% at its extrema, while for  $\Lambda_{\text{NC}} = 2.5$  TeV the modification increases to about 7%. Assuming a conservative experimental sensitivity at the 5% level for measurements of this observable at future  $e^+e^-$  colliders, these results indicate that the azimuthal distribution could provide a powerful handle for either detecting space-time noncommutative effects or setting meaningful lower bounds on the NC scale at the level of a few TeV.

## 5. Conclusions

In this work we have investigated the phenomenological consequences of space-time noncommutativity in the process  $e^+e^- \rightarrow t\bar{t}$  within the framework of the mNCSM. Focusing on both total and differential observables, we have analyzed how NC effects modify the production rate and angular distributions of top-quark pairs at high-energy lepton colliders.

We first established the kinematical setup and clarified the role played by different choices of the NC deformation tensor. While purely space-space noncommutativity leads to vanishing leading-order corrections for the  $s$ -channel process under consideration, allowing for space-time noncommutativity generates nontrivial and potentially observable effects. Although such deformations are known to induce apparent unitarity-violating behavior at very high energies, we have emphasized that this should be interpreted as a limitation of the effective theory description. Accordingly, our analysis was restricted to energy regimes  $\sqrt{s} \lesssim \Lambda_{\text{NC}}$ , where differential observables remain under perturbative control and provide reliable probes of NC dynamics.

Using a benchmark ‘‘detection threshold’’ criterion, we quantified the sensitivity of future  $e^+e^-$  colliders to the NC scale through total cross-section measurements. We found an approximately linear relation between the threshold center-of-mass energy and the NC scale, which offers a simple and practical guideline for assessing the discovery reach or exclusion potential of a given collider setup. This relation allows null results at a fixed energy to be directly translated into lower bounds on  $\Lambda_{\text{NC}}$ .

We then turned to differential observables, which constitute the most robust signatures of noncommutativity. The polar-angle distribution of the top quark and the associated forward-backward asymmetry were shown to be sensitive to both

transverse and longitudinal deformations of space-time. In particular, longitudinal deformations enhance the forward-backward asymmetry, while transverse deformations tend to reduce it. At multi-TeV center-of-mass energies, percent-level deviations from the SM predictions were found for NC scales in the TeV range, indicating that precision measurements of these observables could either reveal hints of noncommutativity or significantly tighten existing bounds.

Finally, we studied the azimuthal distribution of the top quark, which is flat in the SM but acquires characteristic sinusoidal modulations in the presence of transverse space-time noncommutativity. We showed that these azimuthal modulations can reach several percent at  $\sqrt{s} = 3$  TeV for NC scales of  $\Lambda_{\text{NC}} \sim 2.5\text{--}3$  TeV, making them particularly clean and sensitive probes of noncommutative effects. Given the clean experimental environment, high luminosity, and excellent reconstruction capabilities anticipated at future linear colliders, such measurements appear well within realistic experimental reach.

In summary, our results demonstrate that top-quark pair production at high-energy  $e^+e^-$  colliders provides a powerful and complementary avenue for probing space-time noncommutativity. Differential observables, especially polar and azimuthal angular distributions, emerge as particularly sensitive and theoretically robust probes. Future precision measurements in the top-quark sector therefore have strong potential either to uncover signatures of noncommutative space-time or to push the corresponding NC scale well into the multi-TeV regime.

## Acknowledgments

This work was supported by PRFU research project No. B00L02UN050120230003. The authors gratefully acknowledge financial support from the Algerian Ministry of Higher Education and Scientific Research and the Directorate General for Scientific Research and Technological Development (DGRSDT).

## Appendix A. Feynman rules

Following the formulation of the mNCSM presented in ref. [33], we summarize here the NC Feynman rules relevant for the present work. In particular, we list the vertices involving a fermion-antifermion pair of mass  $m_f$  and a neutral gauge boson,  $ff\gamma$  and  $ffZ$ , including corrections up to first order in the noncommutativity parameter  $\Theta^{\mu\nu}$ , i.e.  $\mathcal{O}(\Theta)$ .

The NC Feynman rule for the vertex  $f(p_{\text{in}}) - f(p_{\text{out}}) - \gamma/Z(k)$ , depicted in figure

8, is given by [33]

$$\mathcal{V}_{ff\gamma} = ieQ_f \left[ \gamma_\mu \left( 1 - \frac{i}{2}(p_{\text{out}}\Theta p_{\text{in}}) \right) + \frac{i}{2}(p_{\text{out}}\Theta)_\mu (\not{p}_{\text{in}} - m_f) + \frac{i}{2}(\Theta p_{\text{in}})_\mu (\not{p}_{\text{out}} - m_f) \right], \quad (\text{A.1a})$$

$$\mathcal{V}_{ffZ} = \frac{ie}{\sin(2\theta_w)} \left[ \gamma_\mu \left( c_V^f - c_A^f \gamma_5 \right) \left( 1 - \frac{i}{2}(p_{\text{out}}\Theta p_{\text{in}}) \right) + \frac{i}{2}(p_{\text{out}}\Theta)_\mu \left( c_V^f + c_A^f \gamma_5 \right) (\not{p}_{\text{in}} - m_f) + \frac{i}{2}(\Theta p_{\text{in}})_\mu (\not{p}_{\text{out}} - m_f) \left( c_V^f - c_A^f \gamma_5 \right) \right], \quad (\text{A.1b})$$

where  $(\Theta p_i)_\mu \equiv \Theta_{\mu\nu} p_i^\nu = -(p_i \Theta)_\mu$ . Here  $p_{\text{in}}$  denotes the momentum of the fermion

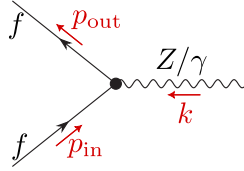


Fig. 8. The  $ff\gamma/Z$  vertex in the mNCSM. The fermion momentum  $p_{\text{in}}$  flows into the vertex and  $p_{\text{out}}$  flows out, while the gauge-boson momentum  $k$  is taken to flow into the vertex.

line entering the vertex, while  $p_{\text{out}}$  corresponds to the momentum of the fermion line leaving the vertex. Fermion momentum flow follows the direction of the fermion line, and the gauge-boson momentum  $k$  is always taken to flow into the vertex. Momentum conservation at the vertex implies  $p_{\text{in}} + k = p_{\text{out}}$ .

For the  $e^+e^-\gamma/Z$  vertex appearing in figure 1, the momenta are identified as  $p_{\text{in}} = p_1$ ,  $p_{\text{out}} = -p_2$ , and  $k = -p_1 - p_2$ . The corresponding vertex factor is sandwiched between Dirac spinors as  $\bar{v}(p_2) \mathcal{V}_{ee\gamma/Z} u(p_1)$ . Making use of the equations of motion,

$$\bar{v}(p_2)(\not{p}_2 + m_e) = 0, \quad (\not{p}_1 - m_e)u(p_1) = 0, \quad (\text{A.2})$$

effectively allows us to replace  $-\not{p}_2 - m_e \rightarrow 0$  and  $\not{p}_1 - m_e \rightarrow 0$  both in the  $\gamma$  and  $Z$  vertices. One thus finds that the terms proportional to  $(\not{p}_{\text{in}} - m_f)$  and  $(\not{p}_{\text{out}} - m_f)$  vanish identically for both the photon and  $Z$  vertices.

An analogous simplification applies to the top-quark vertex, where  $p_{\text{in}} = -p_4$  and  $p_{\text{out}} = p_3$ , and the vertex is inserted between spinors as  $\bar{u}(p_3) \mathcal{V}_{tt\gamma/Z} v(p_4)$ . Using

$$(\not{p}_4 + m_t)v(p_4) = 0, \quad \bar{u}(p_3)(\not{p}_3 - m_t) = 0, \quad (\text{A.3})$$

the momentum-dependent terms of the vertices  $(\not{p}_{\text{in}} - m_f)$  and  $(\not{p}_{\text{out}} - m_f)$  again vanish. Consequently, only the leading  $\gamma_\mu$  terms in each vertex contribute to the amplitudes, as indicated in Eq. (3).

## References

1. ATLAS Collaboration, G. Aad *et al.*, *Phys. Lett. B* **716**, 1 (2012), [arXiv:1207.7214 \[hep-ex\]](https://arxiv.org/abs/1207.7214).
2. CMS Collaboration, S. Chatrchyan *et al.*, *Phys. Lett. B* **716**, 30 (2012), [arXiv:1207.7235 \[hep-ex\]](https://arxiv.org/abs/1207.7235).
3. P. Fayet, *Nucl. Phys. B* **90**, 104 (1975).
4. S. Zaim, A. Boudine, N. Mebarki and M. Moumni, *Rom. J. Phys.* **53**, 445 (2008).
5. I. Antoniadis, *Phys. Lett. B* **246**, 377 (1990).
6. N. Arkani-Hamed, S. Dimopoulos and G. R. Dvali, *Phys. Lett. B* **429**, 263 (1998), [arXiv:hep-ph/9803315](https://arxiv.org/abs/hep-ph/9803315).
7. I. Antoniadis, N. Arkani-Hamed, S. Dimopoulos and G. R. Dvali, *Phys. Lett. B* **436**, 257 (1998), [arXiv:hep-ph/9804398](https://arxiv.org/abs/hep-ph/9804398).
8. T. Appelquist, H.-C. Cheng and B. A. Dobrescu, *Phys. Rev. D* **64**, 035002 (2001), [arXiv:hep-ph/0012100](https://arxiv.org/abs/hep-ph/0012100).
9. A. Connes, *Noncommutative geometry* (Academic Press, 1994).
10. Y. Abe *et al.* (5 2025), [arXiv:2505.11292 \[hep-ex\]](https://arxiv.org/abs/2505.11292).
11. Linear Collider Vision Collaboration, H. Abramowicz *et al.* (3 2025), [arXiv:2503.19983 \[hep-ex\]](https://arxiv.org/abs/2503.19983).
12. E. Adli *et al.* (3 2025), [arXiv:2503.24168 \[physics.acc-ph\]](https://arxiv.org/abs/2503.24168).
13. FCC Collaboration, M. Benedikt *et al.* (4 2025), [arXiv:2505.00272 \[hep-ex\]](https://arxiv.org/abs/2505.00272).
14. CEPC Study Group Collaboration, W. Abdallah *et al.*, *Radiat. Detect. Technol. Methods* **8**, 1 (2024), [arXiv:2312.14363 \[physics.acc-ph\]](https://arxiv.org/abs/2312.14363), [Erratum: Radiat.Detect.Technol.Methods 9, 184–192 (2025)].
15. H. S. Snyder, *Phys. Rev.* **71**, 38 (1947).
16. N. Seiberg and E. Witten, *JHEP* **09**, 032 (1999), [arXiv:hep-th/9908142](https://arxiv.org/abs/hep-th/9908142).
17. N. Seiberg, L. Susskind and N. Toumbas, *JHEP* **06**, 021 (2000), [arXiv:hep-th/0005040](https://arxiv.org/abs/hep-th/0005040).
18. X. Calmet, B. Jurco, P. Schupp, J. Wess and M. Wohlgenannt, *Eur. Phys. J. C* **23**, 363 (2002), [arXiv:hep-ph/0111115](https://arxiv.org/abs/hep-ph/0111115).
19. S. Minwalla, M. Van Raamsdonk and N. Seiberg, *JHEP* **02**, 020 (2000), [arXiv:hep-th/9912072](https://arxiv.org/abs/hep-th/9912072).
20. J. Gomis and T. Mehen, *Nucl. Phys. B* **591**, 265 (2000), [arXiv:hep-th/0005129](https://arxiv.org/abs/hep-th/0005129).
21. M. Van Raamsdonk, *JHEP* **11**, 006 (2001), [arXiv:hep-th/0110093](https://arxiv.org/abs/hep-th/0110093).
22. A. Bichl, J. Grimstrup, H. Grosse, L. Popp, M. Schweda and R. Wulkenhaar, *JHEP* **06**, 013 (2001), [arXiv:hep-th/0104097](https://arxiv.org/abs/hep-th/0104097).
23. J.-H. Huang and Z.-M. Sheng, *Phys. Lett. B* **678**, 250 (2009).
24. W. Behr, N. G. Deshpande, G. Duplancic, P. Schupp, J. Trampetic and J. Wess, *Eur. Phys. J. C* **29**, 441 (2003), [arXiv:hep-ph/0202121](https://arxiv.org/abs/hep-ph/0202121).
25. M. Fisli and N. Mebarki, *Adv. High Energy Phys.* **2020**, 7279627 (2020).
26. L. Ghegai and A. Benslama, *Int. J. Mod. Phys. A* **29**, 1450199 (2014).
27. M. Buric, D. Latas, V. Radovanovic and J. Trampetic, *Phys. Rev. D* **75**, 097701 (2007), [arXiv:hep-ph/0611299](https://arxiv.org/abs/hep-ph/0611299).
28. A. Alboteanu, T. Ohl and R. Ruckl, *Phys. Rev. D* **74**, 096004 (2006), [arXiv:hep-ph/0608155](https://arxiv.org/abs/hep-ph/0608155).
29. T. Ohl and C. Speckner, *Phys. Rev. D* **82**, 116011 (2010), [arXiv:1008.4710 \[hep-ph\]](https://arxiv.org/abs/1008.4710).
30. J. Selvaganapathy, P. K. Das and P. Konar, *Phys. Rev. D* **93**, 116003 (2016), [arXiv:1602.02997 \[hep-ph\]](https://arxiv.org/abs/1602.02997).
31. J. Selvaganapathy, P. Konar and P. K. Das, *JHEP* **06**, 108 (2019), [arXiv:1903.03478 \[hep-ph\]](https://arxiv.org/abs/1903.03478).
32. P. K. Das and A. Prakash, *Int. J. Mod. Phys. A* **28**, 1350004 (2013),

18 *F. Z. Bara, S. Zaiem and Y. Delenda*

[arXiv:1207.1246 \[hep-ph\]](https://arxiv.org/abs/1207.1246).

33. B. Melic, K. Passek-Kumericki, J. Trampetic, P. Schupp and M. Wohlgenannt, *Eur. Phys. J. C* **42**, 499 (2005), [arXiv:hep-ph/0503064](https://arxiv.org/abs/hep-ph/0503064).